Molecular Crystals and Liquid Crystals Science and Technology. Section A. Molecular Crystals and Liquid Crystals

Publication details, including instructions for authors and subscription information:
http://www.tandfonline.com/loi/gmcl19

Experimental Results on the Director Distribution in Hybrid Nematic Films Using A.T.I.R

M. Warenghem [a] , D. Louvergneaux [a] & F. Simoni [b]

[a] Laboratoire de Dynamique et Structure des Matériaux Moléculaires, U.R.A. C.N.R.S. 801; U.S.T.L.; F.59655, VILLE NEUVE D'ASCQ Cedex Laboratoire de Physico-Chimie des Interfaces et Applications Faculté Jean Perrin, Rue Jean Souvraz, SP 18-F-62307, LENS Cedex

[b] Dipartimento di Scienze Fisiche, Università di Napoli, Piazzale Tecchio 80, 80125, NAPOLI, ITALY

Version of record first published: 24 Sep 2006.

To cite this article: M. Warenghem , D. Louvergneaux & F. Simoni (1996): Experimental Results on the Director Distribution in Hybrid Nematic Films Using A.T.I.R, Molecular Crystals and Liquid Crystals Science and Technology. Section A. Molecular Crystals and Liquid Crystals, 282:1, 235-258

To link to this article: http://dx.doi.org/10.1080/10587259608037579

Mol. Cryst. Liq. Cryst., 1996, Vol. 282, pp. 235–258
Reprints available directly from the publisher
Photocopying permitted by license only

EXPERIMENTAL RESULTS ON THE DIRECTOR DISTRIBUTION IN HYBRID NEMATIC FILMS USING A.T.I.R.

M. WARENGHEM, D. LOUVERGNEAUX, F. SIMONI°,
Laboratoire de Dynamique et Structure des Matériaux Moléculaires
U.R.A. C.N.R.S. 801; U.S.T.L.; F.59655, VILLE NEUVE D'ASCQ Cedex
Laboratoire de Physico-Chimie des Interfaces et Applications
Faculté Jean Perrin, Rue Jean Souvraz, SP 18 - F-62307, LENS Cedex
°Dipartimento di Scienze Fisiche; Università di Napoli; Piazzale Tecchio 80
80125 NAPOLI, ITALY

Abstract Using an Attenuated Total Internal Reflection (A.T.I.R.) technique which is herein fully detailed, we have determined the director distribution in some hybrid nematic films at the vicinity of the interface where the nematic is homeotropically aligned. This latter alignment is achieved using two different surfactants: either n-Hexadecyl-Trimethyl-Ammonium-Bromid or lecithin. These experimental measurements are confronted with the results obtained from the elastic theory: a discrepancy close to the interface is observed for the films treated with the lecithin. An exponentially decaying correction to the elastic theory is found to fit the experimental datas.

INTRODUCTION

The bulk distortion of a nematic can be described using the elastic theory due to Frank [1]. The behavior that is obtained from this theory is usually in agreement with the experimental observations. Depending on the degree of accuracy of the experiment, the so-called one constant approximation gives most of the time the correct behavior for the distorted sample. As an actual sample is obviously of finite size, it should be theoretically accounted for the boundary conditions: so did Barrat and Jenkins [2]. To solve the obtained equations, it should be entered an expression for the interfacial energy. Usually, a sine function, known now as the Rapini-Papoular form [3], is fine for most of the case; however this model has been improved to account for more specific

boundary cases [4 - 6]. In addition to the improvement of the surface energy expression itself, it has been accounted for the intriguing K_{13} and K_{24} elastic constants, the associated energies of which can be inserted in the surface terms. The question that arises from these two constants is whether or not they can be responsible for specific effects and/or threrefrom measured. The problem has been solved for the constant K_{24} [7 - 13] but seems to be still wide open for the other term K_{13} due to the mathematical problems that are associated to the minimization of the energy [14 - 17][1]. At this very moment, the feeling for an experimentalist is that the theoretical problem is not yet well posed although improving very fast during these last monthes. A contribution from the experimentalists should be to gather experimental results that are obtained independently of any model.

In several previous papers [18 - 21], it has been demonstrated an experimental method to obtain the director distribution in a distorted nematic film. It consists in processing an equal thickness fringe pattern which can be observed under total internal reflection (A.T.I.R.) conditions. This method is especially well suited to study the distortion close to an interface and the data processing that yields to the distribution uses only the geometrical optics approach and does not require further theoretical model contrarily to some other methods [22, 23].

In this paper, we report the director distributions obtained using this method in the case of an hybrid aligned nematic film and the comparison of the obtained experimental director distribution with that calculated using the usual elastic theory. An hybrid nematic film is a film homeotropically aligned on one side and planarly on the next side. The planar alignment of the studied films has been achieved by unidirectionally rubbing the glass plate that limits the nematic film and the homeotropic alignment by using either lecithin or n-hexadecyltrimethylammoniumbromid (n-HTAB). It is found that one of the used surfactant (lecithin) induces a director distortion close to the interface that is not in agreement with a simple elastic model.

The discrepancy between the experimental results and the elastic theory being not very large but obvious, it seems important to carefully describe the data processing that allowes to determine the director distribution. Therefore this data processing is described in a first part, the experimental results are reported in a second part and the confrontation with the elastic model and a correction that fits the experimental datas are proposed in the third part. In the discussion, it will be considered whether the observed experimental

---

[1]For this specific subject, it is given only some references, the reader should consider the references cited in these papers.

behavior is just an artefact due to the experimental procedure or an experimental evidence for further models.

I. SETUP, GENERAL ANALYSIS AND DATA PROCESSING

I.1 Setup.

The used setup has been already described in the previous papers [18]: it is an usual Total Internal Reflection (T.I.R.) as shown in figure 1. The nematic film is deposited onto the upper face of a dense prism. A low power He-Ne laser beam is reflected at the nematic-prism interface. The reflected intensity is recorded by means of a photosensor which is located at a distance of around 2 meters from the sample with an input aperture of 2 mm^2 (the sensitive surface of the photosensor is 2 cm^2 far away from the input aperture). The angle of incidence can be varied step by step (1/100 or 1/1000 degree) by rotating the mirrors mounted on gimbals; the prism is therefore lifted up or down to illuminate the sample always at the same place. A polariser is inserted in the field to excite either the TE or TM modes. We consider in these studies that the nematic is distorted in the plane of incidence of the probe beam, therefore the TE mode corresponds to the ordinary wave in the nematic, whereas the TM mode excites the extraordinary wave (such an hypothesis can be and is checked during the data processing). Typically an experiment consists in recording the intensity reflected at the sample interface against the angle of incidence, for both polarisations of the beam.

A typical curve is shown in figure 2 where it can be seen the T.I.R. regime on the right side and the transmission regime on the left one. The fringe pattern which is observed in the transmission regime corresponds to an equal thickness fringe pattern between two beams as shown on the figures 3.

I.2 General Analysis.

The informations that can be derived from the reflectivity curves are classified in two parts: first, the limit between TIR and transmission regime containing informations on the interface prism-nematic (on a wavelength scale) and second, the fringe pattern that contains informations on the bulk. After having briefly recalled how the interface can be characterised, we do focus on the second part especially in showing how the fringe pattern can improve the knowledge of the limit in between TIR and transmission regime.

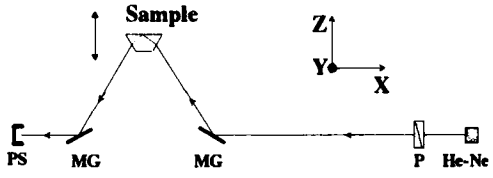

PS: photosensor; P: polariser; MG: mirror gimbal

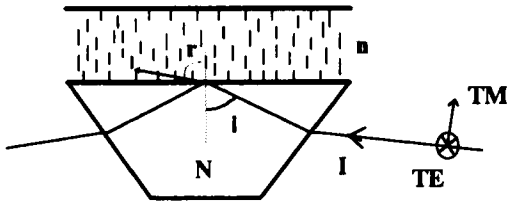

FIGURE 1 A.T.I.R. setup. Up: side view; down: sample closer view.

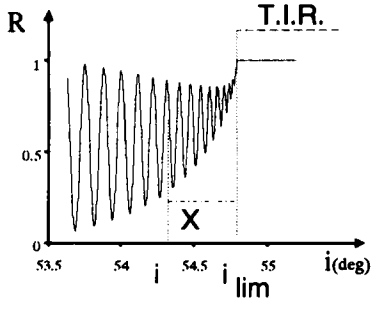

FIGURE 2 General trend of reflectivity curve.

I.2.a. Surface characterisation.

The used setup is an Abbe or Pulfrich refractometer and by applying the Snell-Descartes law to the incidence angle which limits both regimes, one obtain the refractive index of the material deposited onto the prism. In the case of a birefringent material and for our geometry, the TE mode, that is to say the ordinary wave, gives the ordinary index. This index only depends on temperature and by comparing the obtained value with a set of values obtained elsewhere [24], one can deduce the surface temperature and the principal extraordinary index. For the TM mode, the extraordinary ray, we have to

account for the direction of propagation of the energy (and not that of the phase) and the Snell law properly applied writes :

$$N^2 \sin^2(i_l) = n_o^2(T).\sin^2(\theta_s) + n_e^2(T).\sin^2(\theta_s) \qquad 1$$

where θ_S is the surface tilt angle of the optical axis (with respect to the normal to the interface), n_e and n_O are the temperature dependent principal refractive indices of the nematic, i_l is the limit angle between the T.I.R. and transmission regimes and N is the refractive index of the prism. Therefrom, the limit angle measurement for this polarisation gives the surface tilt angle [25,26]. From an experimental point of view, it is not always easy to spot out obviously the limit angle and the accuracy on the measurements of the index and tilt angle depends on how sharp is the limit between both regimes. Later on the text, it will be shown that this accuracy can be improved by using the fringe pattern.

I.2.b. Fringe pattern analysis.

Depending on the polarisation of the probe beam, the nematic can be optically either homogeneous or heterogeneous, that is to say the index is constant or spatially dependent and as a result, the beam is travelling straigthforward or can be deflected. Obviously, for a non-distorted nematic, the refractive index is constant throughout the film whatever the polarisation of the probe beam. In case of a nematic distorted only in a plane, a probe beam travelling in this plane and linearly polarised perpendicular to this plane "sees" a constant refractive index which is the ordinary one, whereas a beam polarised in the plane is travelling through with a refractive index that depends on the direction of the local optical axis with respect to the propagation direction. According to these remarks, the fringe pattern that is visible on the reflectivity curves (leftmost part on figure 2) can be understood and used.

It is an equal thickness fringe pattern and here, we are interested in the situations shown in figure 3 where the probe beam is travelling in the plane of the figure. The first situation is that of an homogeneous nematic film and the associated pattern corresponds to interferences between the beam reflected at the prism-nematic interface and that one which is reflected at the sample upper interface (Fig. 3a). This situation is the same for both polarisations of the probe beam and for either a planar, tilted or homeotropic homogeneous film. The second case is that of a film which is distorted in a plane, with an index gradient perpendicular to the interface and negative (the index decreases with the distance to the interface); the probe beam is travelling in this plane. For a linear polarisation perpendicular to the plane (ordinary ray) the nematic is "seen" as an homogeneous material and the rays that are interfering are shown on the figure 3b as dotted line. For a linear polarisation in the plane, the transmitted beam is deflected

towards the interface and can be totally reflected within the sample, depending on the incidence angle (Fig. 3b, solid line). For an heterogeneous material with a positive index gradient, the situation is the same as in previous case with nevertheless a major difference: there can not be total internal reflection within the sample (Figure 3c).

Experimentally, an hybrid nematic film can not be readily distinguished from an homogeneous planar film. Depending on the anchoring energies and the film thickness, and despite the antagonistic surface treatments the obtained film can be homogeneous, being thinner that the actual critical thickness [27]. Moreover, the reflectivity curves look quite the same for any films, therefore it is neccessary first to check whether or not the studied film is heterogeneous: this is what is done in the first step of the data processing which is detailed in the section 1.3.

In any cases, this data processing is based on the fringe pattern, whose study goes through the phase difference considerations, this is why the next paragraph is devoted to such considerations.

I.2.c Phase difference analysis.

In our configuration, this phase difference between the two beams or the order of interference is expressed as below:

$$\frac{\Phi}{2.\pi} = \frac{1}{\lambda}\int_0^e n(\theta,r).\cos(r).dz + \frac{1}{\lambda}\int_e^0 n(\theta',r').\cos(r').dz + \frac{\Phi_r}{2.\pi} \qquad 2$$

where the first integral corresponds to the part of the transmitted beam going up and the second to that going down, θ and r are respectively the local optical axis tilt angle and local refraction angle with respect to the normal to the interface; e is the limit of the integral that can be either the total thickness d of the film or a part of it. The additionnal constant term ϕ_r (which was not expressed for the sake of simplicity in the previous papers, but accounted for in the processing) corresponds to the phase shifts that occur at the reflections on the different interfaces and in the heterogeneous material. The values of these shifts can readily be deduced from the Fresnel coefficients. The shift is zero for a TE ray totally or partially internally reflected, i.e. incident and reflected beams in the denser material. The shift is still zero for a TM ray partially internally reflected, is π for a TM ray totally internally reflected and π/2 for a TM ray experiencing a total reflection within a gradient index material. We now recall the results obtained on the phase difference including the values of these shifts.

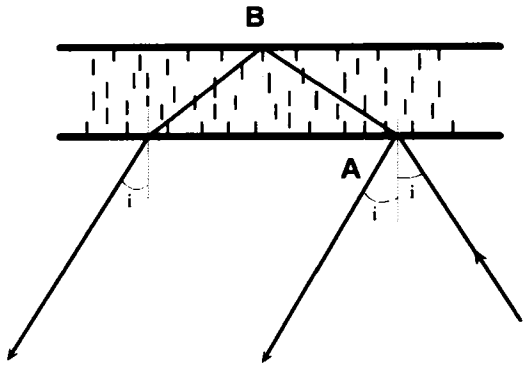

FIGURE 3a. Beams interfering in case of an homogeneous nematic film. The situation is the same for both TE and TM polarisations. An homeotropically aligned film is shown, but such a beam geometry holds on for a planar or tilted homogeneous cell.

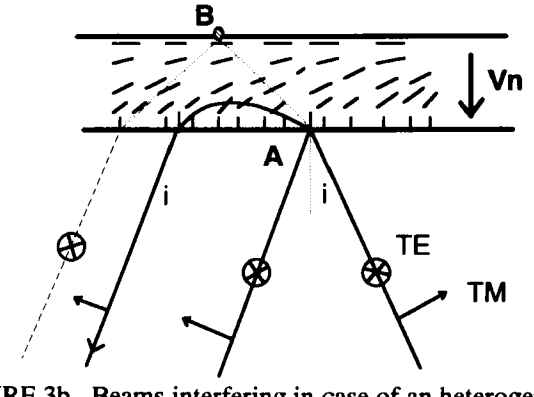

FIGURE 3b Beams interfering in case of an heterogeneous nematic film with an index gradient negative and perpendicular to the interface.

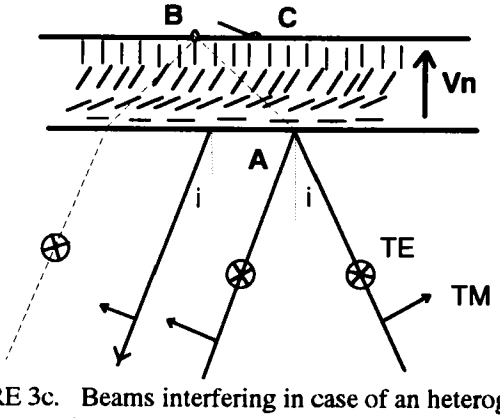

FIGURE 3c. Beams interfering in case of an heterogeneous nematic film with an index gradient positive and perpendicular to the interface.

As it has been pointed out in the reference 18, it is convenient to express the phase difference using the reduced angular abscissa X introduced by Eidner [28, 29] and defined as below:

$$X = \sqrt{N^2.\sin^2(i_{lim}) - N^2.\sin^2(i)} \qquad 3$$

where N is the refractive index of the prism, i is the angle of incidence and i_{lim} is the limit between T.I.R. and transmission regime.

For the ordinary wave (TE mode) and for both in plane distorted and not distorted samples, given that both reflections (A and B, Fig. 3a, 3b) are of the same nature (i.e. internal, the second plate that limits the nematic is a glass with a refractive index which is lower than the ordinary one of the nematic), the total phase shift ϕ_r is zero. The integrals in the expression 2 can be easily calculated and the order of interference is found to be linearly dependent on X, with a slope equal to $2.(d/\lambda)$.

For the extraordinary wave (TM mode) and for an homogeneous film, the phase shift is zero at the first reflection (point A; Fig. 3a) and π at the second (point B, Fig. 3a, the glass index is lower than the extraordinary one of the nematic and the scanned range of angles of incidence is such as the transmission regime is never attained at that point). Again the integrals can be easily calculated and the order of interference is also found linearly dependent on X with a slope equal to $2.(d/\lambda).(n_O/n_e)$ for an homeotropically aligned nematic film and $2.(d/\lambda).(n_e/n_O)$ for a planar sample. In case of a distorted nematic film, the phase shift becomes $\pi/2$ for a ray which is totally reflected due to the index gradient (solid line; Fig. 3b), or zero for a ray which is deflected upwards (Fig. 3.c solid line, it is always a transmission regime at the upper interface). If the calculation of the integrals in the expression 2 is straigthforward in the homogeneous cases, the dependence $\theta(z)$ of the local tilt angle of the director with the position must be known in case of an heterogeneous material. Given that this is exactly what we are looking for, further investigations look endangered. However, the behavior of the phase difference 2 can be evaluated and discussed using a power expansion with respect to the variable X around the origin, i.e. as the angles of incidence are close to the limit angle. To carry out the expansion, it is worthy first to express in a different way the integrals that come in the expression 2. Indeed, using the Snell Descartes law for uniaxial materials and after some easy algebra, the expression 2 can be written as:

$$\frac{\Phi}{2.\pi} = \frac{2.n_o.n_e}{\lambda} \int_{\theta_0}^{\theta_t} \frac{\sqrt{g^2(\theta) - k^2}}{g^2(\theta)} \frac{dz}{d\theta} d\theta + \frac{\Phi_r}{2.\pi} \qquad 4$$

where $g(\theta)$ and k are defined below:

$$g^2(\theta) = n_e^2.\cos^2(\theta) + n_o^2.\sin^2(\theta)$$
$$k^2 = N^2.\sin^2(i) \qquad 5$$

The lower limit θ_0 of the integral 4 is the director tilt angle on the interface (z = 0), whereas the upper limit θ_1 is either the value θ_1 for the director tilt angle at the upper interface or a value which is defined as below:

$$g^2(\theta_l) = k^2 \qquad 6$$

This latter value is the tilt angle at the location where the total internal reflection takes place inside the nematic material. The phase shift ϕ_r is $\pi/2$ for a negative gradient, ie $dz/d\theta$ positive, and is zero for the opposite, i.e. positive gradient, $dz/d\theta$ negative. It is convenient for our purpose to express the phase difference as a function of X.

$$\frac{\Phi}{2\pi} = \frac{2.n_e.n_o}{\lambda}\int_{\theta_0}^{\theta_l}\frac{\sqrt{g^2(\theta)-g^2(\theta_0)+X^2}}{g^2(\theta)}\frac{dz}{d\theta}d\theta + \frac{\Phi_r}{2\pi} \qquad 7$$

The calculation of the expansion is restricted to the second order, due to the experimental values of X that are scanned (typically, X < 0.4):

$$\Phi = \Phi(0) + \left(\frac{d\Phi}{dX}\right)_{X=0}.X + \left(\frac{d^2\Phi}{dX^2}\right)_{X=0}.\frac{X^2}{2} + \ldots. \qquad 8$$

In the expression 7, the derivative $dz/d\theta$ does not depend on X whatever its sign, whereas the upper limit θ_1 depends on it in the case of a total internal reflection within the sample ($dz/d\theta$ positive). The calculation of the different derivatives that come in the expansion 8 is easy to perform, however their value for X = 0 is not obvious.

In the case of an heterogeneous material with a positive index gradient, the upper limit of the integral is θ_1, independent of X and the phase shift ϕ_r is zero. The constant term in (8) is found to be different from zero (9) whereas the first derivative is zero (10) and the second derivative different from zero (11).

$$\frac{\Phi}{2\pi}(0) = \frac{2.n_e.n_o}{\lambda}\int_{\theta_0}^{\theta_l}\frac{\sqrt{g^2(\theta)-g^2(\theta_0)}}{g^2(\theta)}\frac{dz}{d\theta}d\theta \neq 0 \qquad 9$$

$$\frac{1}{2\pi}\left(\frac{d\Phi}{dX}\right)_{X=0} = \lim_{X\to 0}\frac{2.n_e.n_o}{\lambda}\int_{\theta_0}^{\theta_l}\frac{X}{g^2(\theta).\sqrt{g^2(\theta)-g^2(\theta_0)+X^2}}\frac{dz}{d\theta}d\theta = 0 \qquad 10$$

$$\frac{1}{2\pi}\left(\frac{d^2\Phi}{dX^2}\right)_{X=0} = \frac{2.n_e.n_o}{\lambda}\int_{\theta_0}^{\theta_l}\frac{1}{g^2(\theta).\sqrt{g^2(\theta)-g^2(\theta_0)}}\frac{dz}{d\theta}d\theta \neq 0 \qquad 11$$

Finally, the phase difference in this case has a parabolic behavior:

$$\frac{\Phi}{2\pi} = C + K.X^2 + ... \qquad 12$$

In case of a negative gradient, the phase shift is $\pi/2$, the upper limit of the integral depends on X -it is noted θ_X-, the limit X going to zero being equivalent to the upper limit of the integral going to the lower limit $(\theta_X \to \theta_0)$. The constant term is easy to determine: it is given below :

$$\frac{\Phi}{2\pi}(0) = \lim_{\theta_X \to \theta_0} \frac{2.n_e.n_o}{\lambda} \int_{\theta_0}^{\theta_X} \frac{\sqrt{g^2(\theta) - g^2(\theta_0)}}{g^2(\theta)} \frac{dz}{d\theta} d\theta = 0 \qquad 13$$

The first and second derivatives are also easy to calculate, although leading to more complicated expressions, however their limits for X going to zero are undetermined (the expression for the first derivative is given in 14).

$$\frac{1}{2\pi}\left(\frac{d\Phi}{dX}\right)_{X=0} = \lim_{X=0} \frac{2.n_e.n_o}{\lambda} \int_{\theta_0}^{\theta_X} \frac{X}{g^2(\theta).\sqrt{g^2(\theta) - g^2(\theta_0) + X^2}} \frac{dz}{d\theta} d\theta \qquad 14$$

The reason why these derivatives are undetermined for X going to zero is connected to the fact that at the place where the beam is totally reflected, it is travelling parallel to the interface and "never come back", therefore it is illusive to calculate a phase difference, at least in the frame of the geometrical optics. The general behavior is therefore given by:

$$\frac{\Phi}{2\pi} = A.X + K.X^2 + ... + \frac{1}{4} \qquad 15$$

The important result is that the constant term does not exist in such a case, except the 1/4 constant due to the phase difference at the reflexions.

It is worth noticing that to obtain more informations on the values for A and K in 15, one can go further by simulating the phase difference using a computer: it only knows functions defined by pieces and the discontinuity is artificially ignored. However it should be feed with an expression for $dz/d\theta$, in other words, a model for the distortion we are looking for is required. We have performed such simulations using the elastic theory and it is found that the behavior of the phase difference is rather parabolic (A = 0). Anyway, such a result has not been introduced in our processing. We have only used only the main result which is a zero constant term for negative index gradient and a non zero value for positive index gradient, except the constant terms due to the phase difference at the reflexions. All these results are summarised on the table 1, they are also used in the data processing which is now detailed.

TE polarisation	
Homogeneous and **Heterogeneous**	$\frac{\Phi}{2\pi} = 2\frac{d}{\lambda}X$
TM polarisation	
Homogeneous	
Planar	$\frac{\Phi}{2\pi} = 2\frac{d}{\lambda}\frac{n_e}{n_o}X + \frac{1}{2}$
Homeotropic	$\frac{\Phi}{2\pi} = 2\frac{d}{\lambda}\frac{n_o}{n_e}X + \frac{1}{2}$
Tilted	$\frac{\Phi}{2\pi} = 2\frac{d}{\lambda}\frac{n_o n_e}{n^2}X + \frac{1}{2}$
Heterogeneous	
gradient negative	$\frac{\Phi}{2\pi} = K.X^2 + ... + \frac{1}{4}$
gradient positive	$\frac{\Phi}{2\pi} = C + K.X^2 + ...$

Table 1. Calculated dependence on X of the phase difference under different geometries. It is always a linear dependence except for an heterogeneous medium probed with the TM mode.

I.3. Data Processing.

The processing itself consists in three steps: first to build up the curve $\Phi(X)$ to determine whether or not the film is distorted, second to improve the accuracy on the surface parameters and third building up the director distribution $\theta(z)$ function.

I.3.a. First step: distorted or not?

In a fringe pattern, the minima of intensity correspond to orders of interference which are half integers and from a minimum to the next one, the order of interference changes by one unity. Therefore, the abscissa i_k of the k^{th} minimum starting from the limit angle is measured, the associated X_k is calculated using 3 and put on the x-axis together with the corresponding half integer k+1/2 on the y-axis. At this stage, the absolute value for the order of interference can be disregarded (but it is actually

accounted for), the constant additionnal value due to the phase shift associated to the reflexions as well: what is important is the trend of the obtained curve, is it a straight line or a curved one? This question is solved by fitting the data with a polynomial restricted to the second order (usual polynomial least means square fit).

We first process the ordinary reflectivity curve (TE mode): according to the results summarised on the table 1, we should find a straight line; if it is not the case, that means that the director is tilted out of the plane of incidence and such a sample is disregarded. If it is a line, the slope gives us the actual thickness of the film. Second we process in the same way the extraordinary reflectivity curve (TM mode): if one obtains a line that means the film is unperturbed and on the contrary if it is not, it means that there exists a gradient. Before studying this gradient, the parameters such as the actual thickness, ordinary and extraordinary indices are determined with a better accuracy: this is the second step of the processing.

I.3.b. Second step: improving accuracy.

We now focus on the behavior of the curve $\Phi/2\pi(X)$ next to the origin and the absolute value for the order of interference. According to the results summarised on the table 1, the curve should tend towards zero with X for the TE curves. To fill up this condition, there are two quantities which can be adjusted: first the absolute value for the order of interference and second the abscissa for the limit angle. The former changes the order of interference at the origin (i.e. for X going to zero) only step by step whereas a modification of the latter induces a continuous change. Therefore using these two possibilities, the condition on the order of interference at the origin can be filled up quite accurately. Both the abscissa of the minima on the reflectivity curve and the limit angle are requested to calculate the X_k values. If the former can be obtained very accurately (better than 1/100 degree), the abscissa for the limit angle is not always so easy to spot out, lowering the accuracy for the associated X_k value. By changing the abscissa of the limit angle, one changes the whole set of values X_k and therefrom the position of the order of interference on the y-axis for $X = 0$. The routine entered in the computer consists in scanning a range of acceptable abscissa for the limit angle, building up the $\Phi(X)$ curve for each of these abscissa and selecting the value that leads to a curve filling the origin condition. This is done for different absolute values for the order of interference, leading to a set of limit angle abscissa which satisfy the origin condition, these abscissa are plotted on the experimental curve and the right value for the limit angle abscissa becomes obvious as shown on the figures 5 and 6. Using such a procedure, one find out a very accurate value for the abscissa, better than 1/100 of degree, leading to very accurate ordinary index (10^{-4}). The slope of the final $\Phi/2\pi(X)$ curve leads to an accurate determination of an average of the thickness of the film over

the probe beam area. It is very important to notice that it is not a very accurate measurement of the thickness (as it has been stated in an other paper[30]): these accuracies concern only the average of the thickness, the same remark holds on for the index. One also find the absolute value for the order of interference. The same routine is applied for the TM mode curves with more success, due to the fact that usually the limit angle for these curves are not really very sharp (Figure 6). The lone difference is in the origin condition, due to the additional phase shift (cf. Table 1). The accurate limit angle abscissa leads to a better determination for the tilt angle, but as it has already been shown, the next step of the processing do not require such an accurate value: it also finds it out precisely.

I.3.c. Third step: Director distribution.

As the film is found to be distorted, a more sophisticated data processing can be used [31, 32]. It allows to obtain the director distribution within the sample from our experimental curves without theoretical model. It should be noticed that the processing converges only if the film is distorted and checking the sample as presented above is necessary. This bulk distortion determination is presented in an another paper [19, 32] and will not be detailed again.

On the experimental curve, the abscissa i_j of the j^{th} extremum can be measured and using respectively the relations 5 and 6, the associated k_j and θ_j values can be calculated. Remembering that the order of interference is half an integer for a minimum of the reflected intensity, the relation 2 is applied to the p^{th} minimum and the integral is split using the different θ_j values calculated as described above, yielding to the relation 16 :

$$\frac{\Phi_p}{2\pi} = p - 1/2 = \frac{2.n_e.n_o}{\lambda} \sum_{j=0}^{p-1} \left[\int_{\theta_j}^{\theta_{j+1}} \frac{\sqrt{g^2(\theta) - k_p^2}}{g^2(\theta)} \cdot z.d\theta \right] \qquad 16$$

Experimentally, the two angles θ_j and θ_{j+1} are very close together and a linear approximation for the function $z(\theta)$ in this range can reasonnably be used. Therefrom, the derivative $\dot{z}$ that comes in the integral can be considered as a constant, noted $\dot{z}_j$ and pulled out of this integral: this yields to the expression:

$$p - 1/2 = \frac{2.n_e.n_o}{\lambda} \sum_{j=0}^{p-1} \dot{z}_j \left[\int_{\theta_j}^{\theta_{j+1}} \frac{\sqrt{g^2(\theta) - k_p^2}}{g^2(\theta)} .d\theta \right] \qquad 17$$

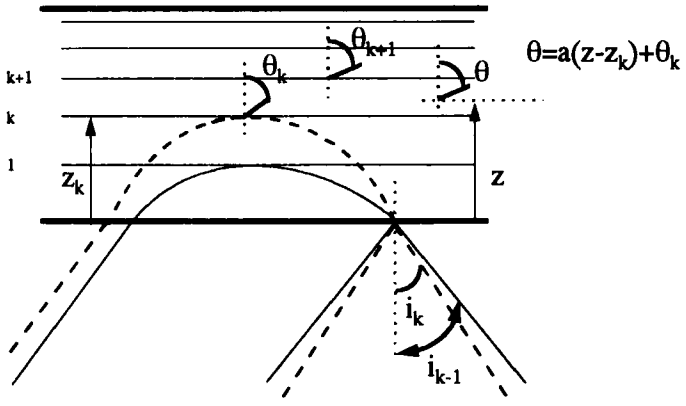

Figure 4 : To obtain the director distribution function, the sample is artificially layered and within each layer, the tilt angle is linearised. The layering is only defined by the angles θ_k that lead to the minima of intensity in the interference pattern. The associated positions z_k are determined by solving a linear system of equations.

The integral now only depends on θ and can be calculated. It is noted $I_{j,p}$ and the relation 17 writes down:

$$p - 1/2 = \frac{2.n_e.n_o}{\lambda} \sum_{j=0}^{p-1} \dot{z}_j . I_{j,p} \qquad 18$$

Applying now this relation to the first extremum, the second and so on up to the p^{th} extremum, a linear system is obtained (19). This system can be solved to give the local derivatives $\dot{z}_j$ and consequently the function $\theta(z)$ itself is readily obtained. The required integration constant is the surface tilt angle of the director and is obtained by measuring the angle of incidence, limit between the T.I.R. and the transmission regimes [19].

$$\begin{aligned}
&\frac{\lambda}{2.n_e.n_o} 0.5 = \dot{z}_0 . I_{0,1} \\
&\frac{\lambda}{2.n_e.n_o} 1.5 = \dot{z}_0 . I_{0,2} + \dot{z}_1 . I_{1,2} \\
&\vdots \\
&\frac{\lambda}{2.n_e.n_o} (p - 1/2) = \dot{z}_0 . I_{0,p} + \cdots + \dot{z}_{p-1} . I_{p-1,p}
\end{aligned} \qquad 19$$

This technique has been used to study the director reorientation of an homeotropically aligned nematic film under an optical field [20, 21], we now present the results obtained in case of hybrid nematic films.

2. EXPERIMENTAL RESULTS.

The Liquid Crystal that has been used is the well known 5CB, compound for which we have measured the values of principal indices versus wavelength and temperature [24]. An hybrid nematic film is a film with two antagonistic alignments: in our case, the homeotropic alignment is imposed on the prism side whereas the planar one is on the next boundary which is an usual glass plate (microscope slide). This planar alignment was achieved by an unidirectionnal rubbing (diamond paste; 1/4 μm grain) and the homeotropic alignment was produced by using two different surfactants: the usual n-hexadecyl trimethyl ammonium bromid (HTAB) and the lecithin. Both surfactants are solved in alcohol or chloroform, deposited onto the prism and the solvent is naturally evaporated, with no further external action. We have prepared in this way 5 films using the HTAB and 4 films using the lecithin, varying the pressure of rubbing and the concentration of these surfactants in order to have different anchoring energies for each films. In addition, the thickness of the lecithin treated samples can be varied by means of piezoelectric devices. The obtained thicknesses are in the range 14 to 140 micrometers. For each films, both TE and TM reflectivity curves for different thicknesses have been recorded. We have selected few curves to illustrate the processing.

On Figure 5 , is shown the reflectivity curve we have recorded for the TE polarisation. From the limit angle, we have deduced the ordinary refractive index and therefrom we have calculated the surface temperature and the extraordinary principal index using the set of values that we measured using an extra experiment [24].

From the TM mode (Figure 6), we have deduced the actual extraordinary index and we have determined the surface tilt angle using the relation 1, which is about 11 degrees in this case. The different values obtained for this angle are discussed later on the text.

For the TE polarisation and the corresponding $\phi(X)$ curve, we have obtained a straight line and we have deduced the thickness of the sample which is about 63 micrometers in this case (Figure 7, left).

For the TM mode and the corresponding $\phi(X)$ curve, we get the information that the film was heterogeneous as a parabolic curve is found and not a straight line (Figure 7, right).

Finally, we have applied the procedure that allows us to build up the director distribution function and the result is shown on the Figure 8 . We have proceeded in the same way for all the films that were achieved. The well marked curvature that is observed next to the interface is obtained for all the films treated with lecithin and is less obvious for the others. The usual elastic theory gives a behavior which is linear in the one constant

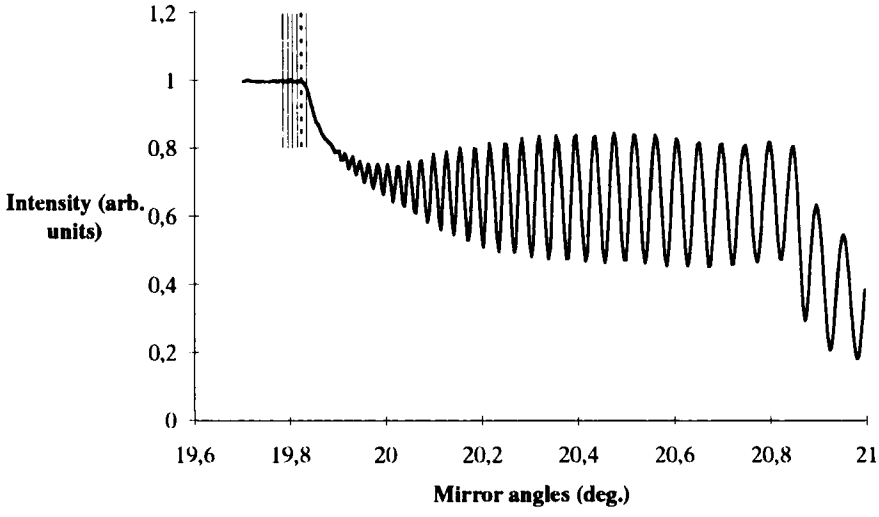

Figure 5 : Reflectivity curve for one film and the TE polarisation. The value of the ordinary index is deduced from the abscissa of the limit angle (n_O = 1.5309), the surface temperature (T = 25.2 °C) and the extraordinary index (n_e = 1.7098) have been deduced from the data set of index versus temperature. The vertical segments around the limit angle correspond to the different limit angles that fullfill the origin condition (see text).

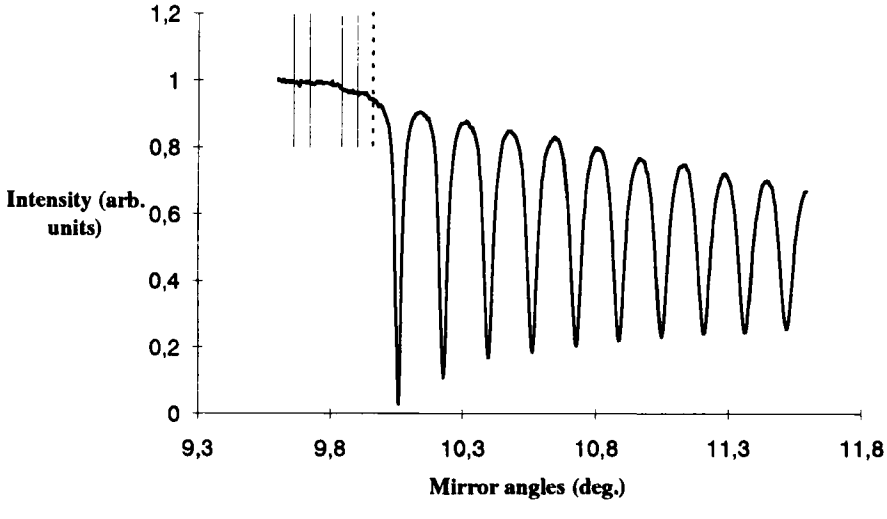

Figure 6: Reflectivity curve for one film and the TM polarisation. From the value of the extraordinary index n = 1.7042 we have deduced the surface tilt angle θ_S = 11 degrees. The vertical segments around the limit angle correspond to the different limit angles that fullfill the origin condition (see text).

approximation and slightly curved in the general case but not a curvature in the surface region as marked as that it has been experimentally found. Therefore it is interesting to check whether or not the obtained director distributions enter the elastic model.

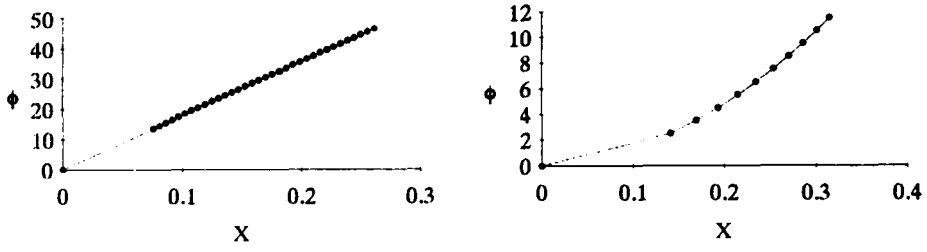

Figure 7: Example of the $\phi(X)$ curve for the TE (left) and the TM (right) polarisations. The parabolic behavior for the TM curve is the signature of an heterogeneous material.

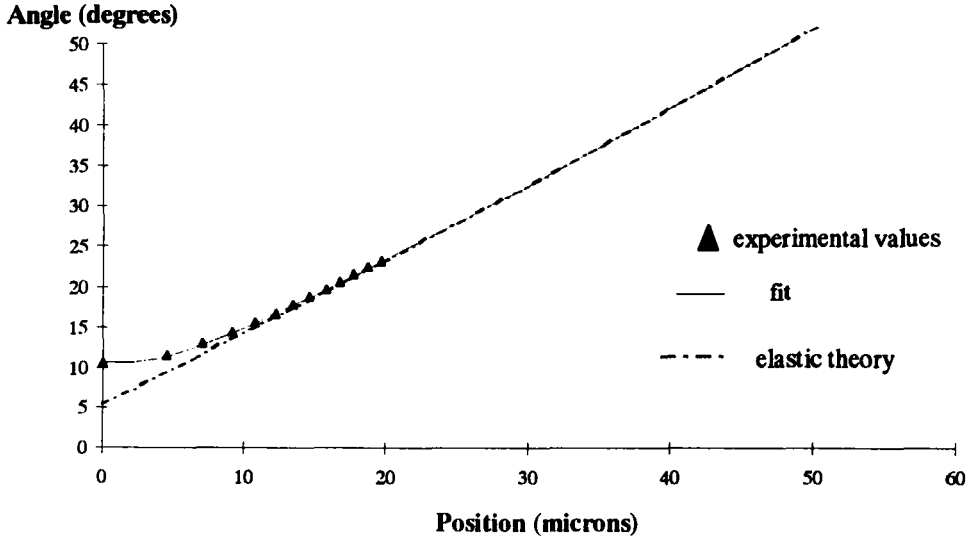

Figure 8 : Comparison between experimental director distribution (triangles) and elastic model (dashed line, from expression 20 in the text). It is impossible to fit the whole set of experimental data points using the expression 20. A possible fit is plotted (solid line, from expression 21 in the text). The height of the triangle indicates the accuracy on the angle.

3. COMPARISON WITH THE ELASTIC MODEL.

Together with the experimental results, we have plotted the usual distribution for the director in an hybrid nematic film, expressed as:

$$z(\theta) = d.\frac{\int_{\theta_0}^{\theta} \sqrt{1 - h^2 \sin^2(\theta')}.d\theta'}{\int_{\theta_0}^{\theta_1} \sqrt{1 - h^2 \sin^2(\theta')}.d\theta'} \qquad 20$$

where h^2 is the anisotropy of the elastic constants (0.3 for 5CB), d the thickness of the film, θ_0 and θ_1 the surface tilt angles. The values for these angles are obtained from the boundary conditions and depend on the surface energies. Given that these surface energies have not been measured for our samples, both surface tilt angles are used as feed parameters.

For the samples treated with HTAB, the experimental director distribution can be fitted with the elastic model, feeding the expression 20 with appropriate surface tilt angles (around 3 degrees for the homeotropic side and 90 degrees for the planar side, for all the samples).

For the samples treated with the lecithin, it is impossible to find a set of two surface tilt angles (θ_0 and θ_1, homeotropic and planar) for which the elastic model fits the experimental datas. It is only possible to fit the experimental director distribution in the bulk, not next to the surface (Figure 8)

Such a discrepancy has been obtained for each thicknesses of the four lecithin samples. While changing the surface tilt angles, a change of around two degrees on the planar side (θ_1 in formula 20) and only half a degree on the homeotropic side (θ_0 in formula 20) is enough to have an observable misfit between the theoretical curve and the experimental datas. The surface tilt angles on the planar side that have been entered to fit the bulk are in between 85 and 90 degrees for all the studied samples whereas the surface tilt angle on the homeotropic side is changing from a sample to the next one and changing as the thickness of one film is lowered (using piezoelectric devices). It should be noticed that different values for the anisotropy of elastic constants have been tested but the obtained change in the director distribution is definitely not fitting the experimental results.

For the first film, the best fit homeotropic angle is 5 ± 0.5 degree, constant for each studied thicknesses (8 different thicknesses between 30 and 121 μm), this value being the same for the two different areas studied on the same sample. For the second sample, the same result is found with now an angle of 6.5 ± 0.5 degree (11 thicknessses between 16 and 90 μm). For the third film, the angle is now slightly decreasing with increasing thickness: from 7 degrees as the film is 14 μm thick to 5 degrees at 127 μm thick; the same values have been found for a second area studied on the same sample.

Finally for the fourth film, a more significant evolution is found, identical to the third one: from 9 degrees as the film is 26 μm thick to 4 degrees at 125 μm thick.

These values for θ_0 have to be compared with the actual experimental surface tilt angles which exhibit the same behavior as shown on the Figure 9 for all the films, namely a slightly increasing angle with a decreasing thickness .

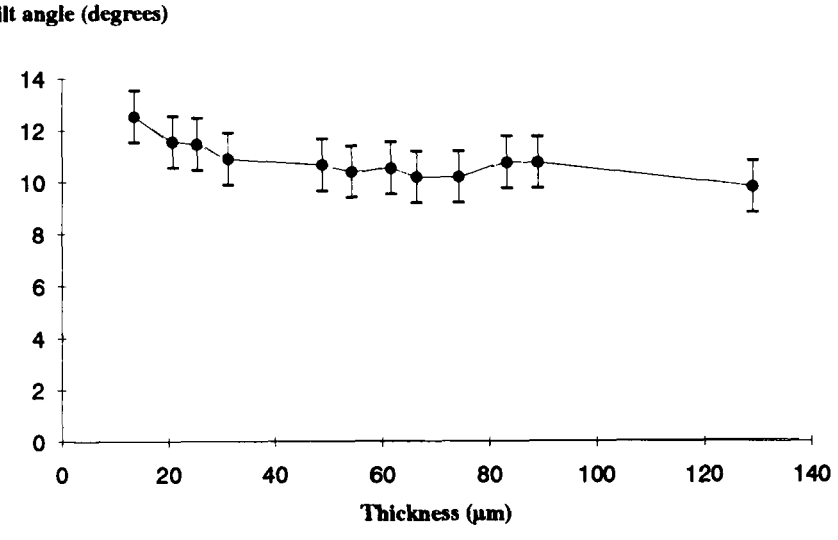

Figure 9. Experimental surface tilt angle on the homeotropic side for a lecithin treated film (film 3).

Such a behavior can be understood in term of anchoring energies: even if these quantities have not been measured, the surface treatments have been achieved in order to have different anchoring energies simply by varying the concentration of the surfactant. For the supposed large anchoring energies (films 1 and 2), it takes a large bulk distortion torque (i.e. a small thickness) to compete with the surface torque and the surface tilt angle is fixed, whereas for the smaller anchoring energies (films 3 and 4) both the bulk and surface torques can equally compete for quite large thicknesses and a variation of the surface tilt angle is more easy.

In addition to this, it is worth noticing that we found for the HTAB treated films some homogeneous samples for thicknesses lower than 30 μm, indicating that such samples was thinner than the so-called critical thickness [27]. For the lecithin treated films, the large distortion energy for the low thicknesses is escaped by a twisted configuration instead of an homogeneous sample.

Anyway, even if these bulk and surface behaviors are not in contradiction with the physical sense of the elastic model, nevertheless the director distribution next to the interface cannot be modelised with that one obtained from the minimisation of the usual Frank bulk energy associated to the usual Rapini Papoular surface energy, which leads to the expression 20.

In order to go further in this surface phenomenon, we tried to fit the obtained distribution with an exponential decay :

$$\theta(z) = \theta_{elast.}(z) + (\theta_s - \theta_0).e^{-\mu.\frac{z}{d}} \qquad 21$$

where $\theta_{elast.}$ is the distribution given by 20, θ_0 the surface tilt angle on the homeotropic side that best fits the bulk distribution and which enters the $\theta_{elast.}$ distribution, θ_s is the actual surface tilt angle measured through the reflectivity curves, d is the actual thickness of the film and μ is a unitless feed parameter.

For each films presenting a discrepancy with the elastic theory, we have checked the best μ parameter: an example is shown on the Figure 10 . For the four studied films, we have found the same quite constant value 19 ±1. This means that the penetration length of the exponential decay is proportional to the sample thickness, with an order of magnitude of the micron.

This surface effect which is not modelized by the usual the theory is obvious but the perturbation is not very large therefore it is important to wonder whether these results are experimental evidences for fuller models or only experimental artefacts. We propose to discuss this in the latest part.

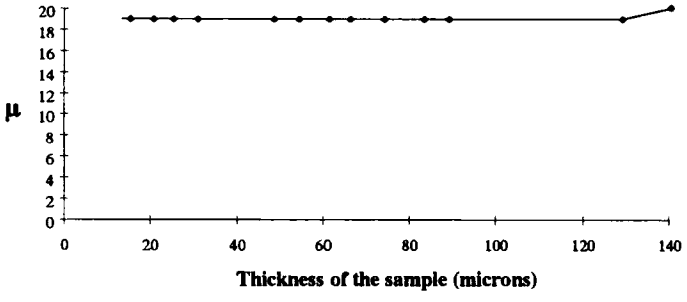

Figure 10. Feeding parameter μ versus thickness of the sample. (accuracy: 1 unit)

4. DISCUSSION.

It is beyond the scope of this purely experimental report to propose a model for what has been observed. We keep going on this experimentalist point of view in giving some comments on the technique and discussing further investigations that have been undertaken, providing the theoreticians with more informations. The additional experiments that have been performed consisted in changing different parameters to check their influence on this surface effect. These experiments are not as comprehensive as that presented above: we were only looking for the existence of the effect.

First of all, we changed the material itself and used the Nematic Liquid Crystal E7 (from Merck): the effect has been observed again, and more important, it has been observed also with the HTAB treated films although less marked than with the lecithin films. However, it can be argued that such compound which is a mixture, contains some 5CB and such an experiment is not really complimentary. Nevertheless, it gives the important information that the effect is not only due to the lecithin.

This observation leads to the following remark : due to the way of preparing the substrate, the surfactant in excess is diffusing in the bulk, inducing a density gradient which in turn can induce an index gradient and this is what might have been observed. Probably such a density gradient exists, but first, the index variation associated with such a gradient is very low (as in any liquid) and second, it should affect both ordinary and extraordinary indices, therefore if it is a measurable effect, it should be seen simultaneously on both TE and TM $\Phi(X)$ curves. Now we found a straight line for the ordinary curve which is the signature of a constant index and a curved line for the extraordinary curve which is the signature of a non constant index. As a result, what have been observed is something else.

However, such density gradient can induce a surface charge distribution and in turn a surface electric field that can reorient the nematic: such an electric field should be perpendicular to the interface and enhance an homeotropic alignment due to the positive dielectric anisotropy of the 5CB. Given that we found a director which is deviating from the homeotropic alignment, a modelisation through some local dipolar interaction looks unlikely, quadrupolar interactions and flexoelectricity looks more promising.

The most important point that has been checked is the validity of one hypothesis the technique is based on: all the data processing is based on an equal thickness fringe pattern analysis, in other words on interferences between two parallel beams. The fringe pattern in the TM mode shows obviously that we are in the presence of a multibeam interferences phenomenon. The data processing uses only the extremum abscissa which are identical whatever the number of path in the interfering system, two or more,

providing that there is a translational symmetry: the lone variable should be the z coordinate. This question has to be checked in two different ways: first to be sure that the sensor is far enough from the sample to record parallel beams and second that the sample itself is homogeneous in the x and y coordinates on a large scale. The first point has been considered in recording and processing curves with a photosensor located at different distances away from the sample: the effect is observed the same way whatever the distance is. The second point has been checked by recording and processing curves for a probe beam analysing different areas of the sample: again no changes have been found as already mentionned in the second part of this paper. Probably the director distribution depends on the x and y coordinates due to some heterogeneity in the surface treatment, but the fact that we found at least two different areas (randomly chosen) that exhibit the surface effect means that it is not due to some particular combination of different non parallel beams interfering within the photosenor with a phase difference that leads to such a reproducible effect.

As a conclusion, we summarize the observations that are reported in this paper. Using an optical technique based on Total Internal Reflection, we have measured the director distribution close to the homeotropic side of an hybrid nematic film. Such an experimental technique do not require any theoretical model and can be used to check some models. We therefore have compared these experimental distributions with that obtained by minimizing the Frank elastic energy associated with the Rapini Papoular surface energies. We found out a misfit between both theoretical and experimental distributions, especially close to the interface, which can be corrected by adding to the elastic model distribution an exponential decay. The penetration length of such a correction is found to be proportional to the thickness of the sample, with an order of magnitude of the micron.

Different models, fuller than the simple elastic one, can be considered to explain the observed behavior: non constant order parameter, second order elasticity which is the K_{13} problem from the Italian group point of view, the K_{13} problem from the Pergamenschik point of view, the flexoelectricity and surface double layer. All these model lead to exponential decays. However, the non constant order parameter is supposed to be volume independent with a characteristic length which is the molecule: this is definitely not what we observed. The same remark holds for the Italian point of view for the K_{13} problem, although this is subsequently developping. The Pergamenschik point of view on this problem seems to be less restrictive in the order of magnitude: the proportionality to the thickness seems not to be in contradiction with the model. The last possible model cited above, namely the flexoelectricity and the surface double layer, seems not convincing: as already mentioned, the dipolar effect acts in the

wrong direction and quadrupolar effect should be involved. However, the order of magnitude (micron) and the volume dependence are correct.

* A part of the experimental results has been presented as poster at E.CL.C.'95 (Bovec, March 1995).

* We are indebted to G. Durand and G. Barbero for all the fruitful discussions.

• This work has been achieved in the frame of the European network "Liquid Crystal: Macroscopic properties". N.ERBCHRXCT930119

REFERENCES

1. F.C. Frank, Dis. Farad. Soc. 29 ,19,(1958)
2. J.T. Jenkins, P.J. Barratt, Quat. J. Mech. Appl Math., 27, 1, 111, (1974)
3. A. Rapini, M. Papoular, J. de Phys., C-4 suppl. 11-12, 30, 54 (1969)
4. E. Dubois-Violette, O. Parodi, J. de Phys., C4 30, 57, (1969)
5. H. Mada, Mol. Cryst. Liq. Cryst., 51, 43, (1991)
6. M. Warenghem, N. Isaert, J. Optics, 16, 1, 37, (1985)
7. G. Barbero, A. Sparavigna, A. Strigazzi, Nuovo Cimento D 12, 1259, (1990)
8. V. M. Pergamenshchik, Phys. Rev., E 48, 1254, (1993) and Phys. Rev., E 49, 934 (1994)
9. D. W. Allender, G. P. Crawford,J.W. Doane, Phys.Rev. Lett., 67, 1442, (1991)
10. S. Zumer, S. Kralj, Liq. Cryst., 12, 4, 613, (1992)
11. R.J. Ondris-Crawford, G.P. Crawford, S. Zumer, J.W. Doane, Phys. Rev. Lett., 70, 194, (1993)
12. R.D. Polak, G.P. Crawford, B.C. Kostival, J.W. Doane, S. Zumer, Phys. Rev. E 49, R978, (1994)
13. A. Sparavigna, O.D. Lavrentovich, A. Strigazzi, Phys. Rev. E49, 1334, (1994)
14. S. Faetti, Liq. Cryst., 15, 6, 807, (1993)
15. G. Barbero, R. Barberi, Physics of Liquid Crystalline Materials, Chapt 8 and 9, Edited by I.C. Khoo and F. Simoni, Gordon and Breach (1991)
16. V. M. Pergamenshchik,P.I.C. Teixeira, T?J? Sluckin, Phys. Rev., E 48, 2, 1265, (1993),
17. O.D. Lavrentovich, V. M. Pergamenshchik, Phys. Rev. Lett., 73, 7, (1994)
18. M. Warenghem, M. Ismaili, D. Hector, J. de Phys. III, 2, 765, (1992).

19. F. Simoni, F. Bloisi, L. Vicari, M. Warenghem, M. Ismaili and D. Hector, Europhys. Lett., 21(2), 189, (1993).
20. M. Warenghem, M. Ismaili, F. Simoni, F. Bloisi, L. Vicari; Mol. Cryst. Liq. Cryst., 251, 43, (1994)
21. M. Warenghem, M. Ismaili, F. Simoni, F. Bloisi, L. Vicari; Mol. Cryst. Liq. Cryst., 251, 61, (1994)
22. C.R. Lavers, J. R. Sambles, Liq.Cryst., 8, 577, (1990)
23. S.J. Elston, Liq.Cryst., 9, 769, (1991)
24. M. Warenghem and G. Joly, Mol. Cryst. Liq. Cryst., 207, 205, (1991).
25. D. Rivière, Y. Levy and C. Imbert, Opt. Comm., 25 (2), 206, (1978).
26. Y. Levy, D. Rivière, C. Imbert and M. Boix, Opt. Comm., 26 (2), 225, (1978).
27. E. Perez, J.E. Proust, L. Ter Minassian-Saraga, E. Mauer, Colloid Polym. Sci., 255, 1003, (1977)
28. K. Eidner, G. Mayer and R. Schuster, Phys. Lett. A, 118(3),149-151, (1986).
29. K. Eidner, G. Mayer and R. Schuster, Phys. Lett. A, 118(3),152-154, (1986).
30. H.A. Van Sprang, Mol. Cryst. Liq. Cryst., 199, 19, (1991).
31. F. Bloisi, L. Vicari, F. Simoni, Nuovo Cimento D, 12, 1273, (1990)
32. F. Bloisi, L. Vicari and F. Simoni, Mol. Cryst. Liq. Cryst., 179, 45, (1990).